Towards Process-Resilient Lignin-Derived Activated Carbons for Hydrogen Storage Applications

Jemma L. Rowlandson,*[†] Karen J. Edler,[‡] Mi Tian,[§] and Valeska P. Ting.*[†]

[†] *Department of Mechanical Engineering, University of Bristol, Bristol, BS8 1TR, United Kingdom.*

[‡] *Department of Chemistry, University of Bath, Bath, BA2 7AY, United Kingdom.*

[§] *Department of Chemical Engineering, University of Bath, Bath, BA2 7AY, United Kingdom.*

* *Email = J.Rowlandson@bristol.ac.uk*

Email = V.Ting@bristol.ac.uk

Abstract

Activated carbons are promising sorbents that have been heavily investigated for the physisorptive storage of hydrogen. The industrial process for production of activated carbons is finely tuned and requires a reliable and uniform feedstock. While the natural biopolymer lignin, a by-product of several industries, has received increasing interest as a potentially sustainable and inexpensive activated carbon feedstock, the ratio of the three aromatic monomers (S, G, and H) in lignin can be heavily affected by the lignin source and growing conditions. The aromatic ratio is known to influence the thermal behavior of the polymer, which could be problematic for production of consistent activated carbons at scale. With the goal of improving the consistency of activated carbons produced from lignins derived from different feedstocks, here we present a route to limiting the influence of lignin feedstock on activated carbon porosity and performance, resulting in a carbonization process that is resilient to changes in lignin source. Two different types of organosolv lignin (representing high S-unit content and high G-unit content feedstocks) were investigated. Resulting activated carbons exhibited a high surface area (> 1000 $m^2 \cdot g^{-1}$) with consistent adsorptive properties and reasonable hydrogen uptake of up to 1.8 wt.% at 1 bar and -196 °C. These findings indicate that low temperature carbonization conditions can be used to produce a consistent carbon material using organosolv lignins from any source, paving the way for more widespread use of lignin in large-scale carbon production.

Keywords:
Nanoporous carbon; hydrogen storage; lignin; activated carbon; porosity

INTRODUCTION

Activated carbons are attractive materials for the physisorptive storage of hydrogen as a sustainable energy carrier.[1,2] Physisorptive hydrogen storage on activated carbon is a well-studied phenomenon. A large material surface area composed of ultramicropores (between 5 and 7 Å) is known to be critical for efficient packing of adsorbed hydrogen at 77 K.[3–8] The preparation of carbons requires pyrolysis of carbonaceous material to form a char with rudimentary porosity, which is enhanced subsequently in a chemical or physical activation procedure.

Lignin, a natural biopolymer derived from lignocellulosic biomass, is a promising activated carbon feedstock due to its low cost, high carbon content, and large-scale availability as a major by-product of the paper pulping and biofuel production industries.[9,10] Lignin has a highly complex structure, which is dependent on the biomass source, growing conditions, and isolation method used to extract the macromolecule. It is formed primarily from three aromatic monomers known as monolignols, namely p-coumaryl, coniferyl, and sinapyl alcohol. These result in the formation of p-hydroxyphenyl (H), guaiacyl (G), and sinapyl (S) residues in the polymer, respectively.[9,11]

Previous work by the authors,[12] and other research groups,[13–17] has demonstrated that pore characteristics of biomass and lignin-derived carbons can be controlled through careful selection of synthesis conditions. However, previous research on biomass-derived carbons has demonstrated the choice of feedstock is also critical to the properties of resulting activated carbon materials,[9,18] affecting the molecular structure of the char, ash and carbon content. In addition, physical changes in the char during heating can affect the char reactivity and activation rate, influencing the development of porosity in activated carbons.[19,20]

Multiple studies have shown the aromatic structure of lignin, determined by the biomass source, affects the thermal behavior of the macromolecule.[21–24] Furthermore, research by Jeon et al.[25] and Carrott et al.[26] have shown activated carbons produced using identical synthesis conditions but using different types of lignin result in varying adsorptive properties, indicating that the chemical and structural heterogeneity exhibited by the different lignin feedstocks influences the activation process. Jeon et al. attributed part of this to a self-activation process within lignin chars, which enhances porosity by the release of low molecular weight volatiles.

Such heterogeneity in lignin is an issue which could preclude its use in large-scale hydrogen storage applications. Potentially vast quantities of activated carbon will be required if on-board vehicular physisorptive hydrogen becomes widespread. Assuming the physisorptive material meets the targets set out by the US Department of Energy (5 kg usable storage capacity with a gravimetric capacity of 7 wt.%)[27] almost 90 tons of material would be required for 50 % of new car registrations in the United Kingdom alone (almost 1.5 million in 2018).[28] Consequently, a cheap and widely available feedstock such as lignin will become critical to meet this demand. However, industrial-scale manufacturing processes for activated carbons are very finely tuned and generally require a consistent feedstock supply to ensure there is no variation in the product quality.[29]

The focus of this work is to show a low temperature carbonization can improve the resilience of the synthesis process to changes in the aromatic lignin structure (determined by the biomass feedstock). Previous studies on lignin-derived activated carbons have utilized lignin isolated both from different feedstocks (affecting the aromatic structure) and using different pulping methods (affecting molecular weight and functional groups) making it challenging to assess the impact of lignin structure on activated carbon properties. A methodical approach is used in this work to isolate and assess any impact of the aromatic structure alone on activated carbon properties.

Biomass feedstocks were chosen to investigate two different types of lignin aromatic structure: grass lignin (flax straw and rice husk) and wood lignin (hemp hurds and eucalyptus chips). To ensure comparability, an identical pulping process was used for extraction. An in-depth investigation into how the synthesis parameters affected activated carbon properties was performed previously by the authors.[12] In this study, low temperature carbonization conditions are employed to restrict porosity development in lignin chars via self-activation, in order to produce carbons with comparable adsorptive performance on activation. We examine the consistency in the adsorptive properties of activated carbons (measured using gas sorption) and in their performance, when applied as a high-value product for physisorptive hydrogen storage. The implications for the industrial scale production of lignin-derived activated carbons are also discussed.

EXPERIMENTAL METHODS

Materials and Methods

The lignocellulosic feedstocks (hemp hurds, eucalyptus chips, flax straw, and rice husk) were provided by MAST Carbon International, Basingstoke. The feedstocks were used as provided, sectioned into pieces up to 3 cm long. All solvents and reagents used were of analytical grade.

Organosolv Lignin Extraction

Lignin was extracted from four different biomass sources using an identical pulping process to obtain high purity starting materials with similar molecular weight and carbon content, to ensure, as far as possible, that the char reactivity and activation rate were unaffected by these parameters. The organosolv extraction method is based on the autocatalytic Alcell process[30] with experimental conditions chosen based on information from several sources.[31–33] Digestion of biomass took place in a knock-out pot (1000 mL) with a sealed inlet and outlet. A suspension of biomass-water-ethanol (100 mL 60:40 ethanol-deionized water solution per 10 g biomass) was heated at 200 °C for 6 h before cooling to room temperature. The delignified fiber and lignin-rich black liquor were separated by filtration, and fibers rinsed with a 60:40 EtOH-DI solution. The filtrate and black liquor were combined, and the ethanol removed under vacuum until the onset of lignin precipitation. Precipitation was achieved by the addition of a 0.1 M sulfuric acid solution to the concentrated liquor (2:1 ratio by volume of acid to liquor) while stirring. Lignin was separated by filtration and rinsed with deionized water until the filtrate pH was neutral, then dried at 55 °C.

Characterization of Lignin

Thorough compositional analysis of lignin (acid-soluble lignin, acid-insoluble lignin, sugars, and ash) was performed by Celignis Analytical, IE using wet chemical methods.[34] The composition was analyzed in duplicate with the mean values reported. Elemental analysis of lignins (C, H, N, S) was performed at the University of Bristol Microanalytical Laboratory, UK using combustion. The O content was determined by difference.

Gel permeation chromatography (GPC) was used to determine the molecular weight and polydispersity of lignin samples. Acetylation of lignin to enable dissolution in tetrahydrofuran (THF) was not required. Samples were dissolved in a THF+LiBr (0.1 wt.%) solution at a concentration of 2 $mg \cdot mL^{-1}$ then passed through a 20 µm polytetrafluorethylene (PTFE) filter. GPC analysis was performed on an Agilent Technologies 1260 Infinity instrument with a flow rate of 1 $mL \cdot min^{-1}$ at 35 °C. THF was used as the eluent and samples were referenced against a

polystyrene standard. Characterization of lignin molecular weight is known to be problematic and absolute values should be used with caution.[21,35,36] Consequently, in this work, the lignin molecular weights were measured in triplicate, and the mean values are reported.

Two-dimensional (2D) ^{1}H-^{13}C HSQC nuclear magnetic resonance (NMR) spectra were acquired on a Bruker Advance III NMR spectrometer operating at 500.13 MHz for ^{1}H and 125.77 MHz for ^{13}C. Lignin samples (ca. 60 mg) were dissolved in dimethyl sulfoxide-d_6. Spectra were acquired using a spectral width of -40 ppm to +180 ppm for ^{13}C, and -1.28 ppm to +10.68 ppm for ^{1}H. The standard Bruker pulse sequence hsqcedetgpsp.3 was used with 128 transients for 256 increments and a TD of 1024 in the F2 direction. Data acquisition and processing were performed using Topspin 2.1. HSQC cross-peak intensities were analyzed using a semi-quantitative method, as described by del Rio et al. and Wen et al.[37,38] The S/G-ratio was determined from peaks in the aromatic region (δ_C/δ_H 95-140 ppm/6.0-7.7 ppm). The $C_{2,6}$-$H_{2,6}$ peak correlating to S-units and the C_2-H_2 plus C_6-H_6 peaks correlating to G-units were used to calculate the S/G-ratio. The same area was integrated over all spectra using the MestReNova software. Cross-peaks were assigned using literature data.[32,35,37–40] Duplicate spectra were collected with the mean integral values reported.

Activated Carbon Preparation

The organosolv-extracted lignin materials were used as activated carbon feedstocks. Pyrolysis and activation of the lignin materials were performed in a horizontal tube furnace (Lenton, LTF 12/75/750) fitted with a digital PID controller (3216CC). The furnace contained a separate alumina work tube fitted with gas-tight end seals. Mass flow controllers (Bronkhorst, EL-FLOW), calibrated using a correlated flow meter (Cole Parmer, 32044-14), were used to control the flow rate of gas into the furnace. PureShield argon (Air Products, 99.998 % purity) at a flow rate of 500 mL·min^{-1} was used as the inert furnace gas, and a heating rate of 5 °C·min^{-1} was used throughout.

The lignin (3 g) was placed in an alumina combustion boat (20 mL capacity) and inserted into the center of the furnace. The furnace was purged with argon for 30 min at room temperature, before heating to 105 °C and held for a further 30 min. The sample was heated from 105 °C to 350 °C and held at temperature for 30 min, before cooling to room temperature. The resulting char was ground and passed through a 35-mesh sieve (500 µm) prior to activation. The ground char (1 g) was heated to the activation temperature of 1000 °C under argon using the same method as the char pyrolysis. At 1000 °C the furnace gas was switched to carbon dioxide (Air Products, 99.999 % purity) at 100 mL·min^{-1} for 50-60 min, then cooled to room temperature in

an argon atmosphere. Physical activation with CO_2 was chosen as the focus of this work due to the lower environmental impact of this process in comparison with chemical activation.[41,42]

Activated Carbon Characterization

Lignin-derived chars and activated carbons were characterized by gas sorption analysis using a 3Flex analyzer from Micromeritics. Nitrogen (Air Products, 99.999 %) at -196 °C and carbon dioxide (Air Products, 99.999 %) at 0 °C were used as the adsorptive gases. Prior to analysis, chars (1 g) and carbons (100 mg) were degassed at 250 °C and 300 °C, respectively, for 4 h at 10^{-7} mbar vacuum. All isotherm data were collected using filler rods from p/p_0 10^{-8} - 1 for N_2 and p/p_0 10^{-5} - 10^{-2} for CO_2. The adsorptive uptake of lignin-derived chars (prior to activation) was determined using a combination of N_2 and CO_2 sorption. Adsorptive parameters and pore size distributions for lignin-derived activated carbons were calculated from N_2 isotherms. Repeat measurements of the upper N_2 isotherm (p/p_0 ~ 0.1-1.0) were performed for all four lignin carbons and of the full N_2 isotherm (p/p_0 ~ 10^{-7}-1.0) for rice husk and hemp lignin carbons. The total pore volume was obtained from the isotherm plateau and the micropore volume and micropore surface area using the t-plot method, according to ISO 15901-3.[43] The BET surface area was calculated according to the procedure from ISO 9277:2010.[44] The Rouquerol correction was applied with the range p/p_0 0.01-0.03 used to calculate the BET surface area. Pore size distributions (PSDs) were calculated by the fitting of two-dimensional non-linear density functional theory (2D-NLDFT) kernels to the N_2 isotherms using 3Flex (Micromeritics) software. A graphitic slit pore shape was assumed with a pore aspect ratio of 4 or 6 chosen to minimize the standard deviation of fit between the model and experimental data. The volume-weighted average pore size was calculated from PSDs according to Laudisio et al.[45]

Powder X-ray diffraction (XRD) patterns of lignin-derived activated carbons were collected in duplicate using a Bruker D8 Advance Diffractometer using Cu-Kα radiation (λ = 1.54 Å, 40 kW, 40 mA) with a step size of 0.05° (2 s per step) and from 10° 2θ to 80° 2θ. Samples were placed on a silicon sample holder, which was rotated throughout the experiment (30 rpm at 0.5 rps) at room temperature. A background spectrum of the sample holder was recorded and subtracted from the activated carbon data. Raman spectra were recorded in triplicate for activated carbons on a Renishaw inVia Raman spectrometer using a 514.5 nm Ar laser excitation at 1 % power to prevent thermal degradation. Spectra were recorded for 30 s from 1000 cm^{-1} to 3200 cm^{-1}. Cosmic radiation removal was performed prior to baseline correction and peak fitting assuming 4 Voigt-profile peaks. X-ray photoelectron spectroscopy (XPS) of

the lignin-derived activated carbons was carried out at the Bristol NanoESCA Facility. Spectra were acquired using Al Kα (1486.7 eV) monochromatic x-rays. Surveys were acquired with 50 eV pass energy and the C1s with 20 eV pass energy.

Uptake of Hydrogen

Lignin-derived carbon powders and an industrially produced carbon TE7 (MAST Carbon International) were characterized by sorption of hydrogen (Air Products, 99.999 %) at -196 °C using a 3Flex volumetric gas sorption analyzer by Micromeritics. Before analysis, carbons (100 mg) were degassed at 300 °C for 4 hours under dynamic 10^{-7} mbar vacuum. Isotherm data were collected using filler rods and using absolute pressure dosing from 5 mbar to 900 mbar. Helium was used to calculate the free space following isotherm collection. The gravimetric uptake of hydrogen was calculated from the excess hydrogen adsorption in moles (n_a), the molar mass of hydrogen (M_H), and the dry, degassed carbon mass (m_{carbon}):[46]

$$H_2\ uptake\ (wt.\%) = \left(\frac{n_a M_H}{m_{carbon} + n_a M_H}\right) \times 100 \qquad (1)$$

RESULTS AND DISCUSSION

Comparison of Lignin Structure

Lignin was successfully isolated from four biomass feedstocks (rice husk, flax straw, hemp hurds, and eucalyptus chips) for activated carbon preparation. The organosolv pulping process was chosen because it results in lignins with less modification in comparison to other isolation methods, to ensure, as far as possible, that any effect of the aromatic composition on carbon porosity was studied in isolation. Extensive characterization of the lignin purity, molecular weight, and aromatic composition were performed using wet chemical methods, gel permeation chromatography (GPC) and 2D HSQC NMR ^{1}H-^{13}C analysis.

Characterization of lignin composition confirmed that, overall, materials were of high purity (>88±1 wt.%) with low levels of ash (<1.2±0.5 wt.%) and sugars (<2.1±0.1 wt.%). Notably, rice husk lignin exhibited a slightly elevated ash (1.2 wt.%) and sugars content (2.1 wt.%) compared to the other lignins (ash and sugars range at 0.4-0.9 wt.%), resulting in a small reduction in total lignin content (88 wt.% compared to 93-96 wt.% for the other lignins). Elemental analysis revealed the lignins were primarily composed of carbon, oxygen, and hydrogen in a ratio of approximately 60:30:5. The lignin materials studied contained small amounts of nitrogen and sulfur (<1 wt.%) resulting from the precipitation procedure. GPC analysis determined all materials exhibited similar molecular weight values (M_n= 900-

1100±60 g·mol^{-1}, M_w= 1300-1600±170 g·mol^{-1}), which are within the range expected for organosolv lignins.[31,35,47,48] See **Table S1** in *Supplementary Information* for a full list of characterization data.

The aromatic structure of lignin is commonly described by the ratio of syringyl to guaiacyl monolignols, known as the S/G-ratio.[32,35,40,49,50] **Figure 1** illustrates the S/G-ratio for the four lignins investigated, derived from the integration of known cross-peaks in 2D NMR spectra (see **Figure S1** in *Supplementary Information*). From the S/G-ratio, the samples were divided into two classes: high S/G-lignin (from hemp and eucalyptus) and low S/G-lignin (from rice husk and flax). The combination of characterization techniques in this work confirmed that the four lignin materials were of high purity with a similar elemental composition and comparable molecular weight values but differed in the ratio of aromatic units that make up the macromolecule. Consequently, these lignins were used to discern whether the aromatic composition has any influence on activated carbon porosity.

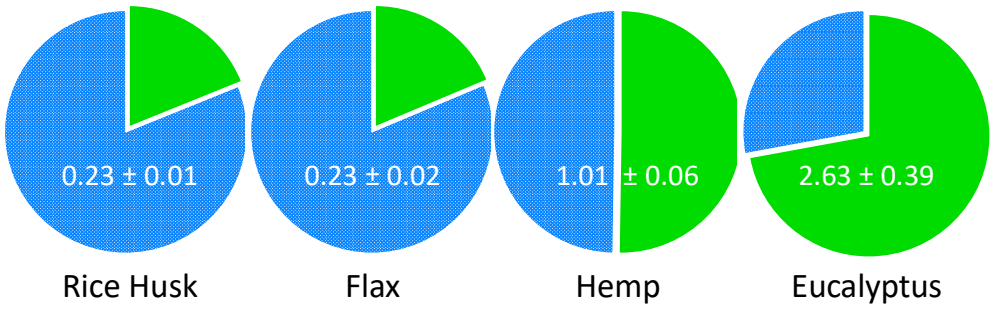

Figure 1. Pie charts illustrating the mean ratio of syringyl (▬) to guaiacyl (▩) units as calculated from 2D-NMR integrals. The S/G-ratio values were calculated from the integrals of at least two different spectra. Uncertainty values represent the largest deviation between measurements and the mean value.

Influence of Aromatic Lignin Structure on Activated Carbon Properties

Carbonization conditions employed in the literature range from a temperature of 350 to 1000 °C with a 30 to 240 min dwell time.[14,51–54] Low temperature carbonization conditions (350 °C for 30 min under argon) were employed here to convert organosolv lignins to chars, forming stand-alone carbon monoliths (**Figure S2**, *Supplementary Information*). These conditions were chosen to limit the formation of char porosity for production of consistent activation carbon materials. Chars were subsequently activated using CO_2. The burn-off levels of the chars and activated carbons were used as a measure for the degree of activation and are listed in **Table 1**.[55,56] Repetition of the carbonization and activation procedure for rice husk and hemp lignin-derived carbons revealed excellent repeatability with burn-off values within ± 1 wt.%. To ensure only the effect of aromatic lignin structure on activated carbon properties was examined, rather than the effect of burn-off,[57] the lignin-derived chars and carbons in this work

were prepared to a consistent burn-off level, ~40 wt.% and ~55 wt.%, respectively. The rice husk lignin activated carbon exhibited an increased burn-off rate compared to the other lignins and required a shortened activation time of 50 min. This enhanced rate can be attributed to increased reactivity resulting from the elevated sugar and ash contents.

Table 1. Burn-off levels for lignin-derived chars (carbonized at 350 °C for 30 min under argon) and activated carbons (using CO_2 and activated at 1000 °C for 60 min, unless otherwise stated).

Lignin feedstock	Burn-off (wt.%)	
	Char	Activated carbon
Rice husk	39	56[a]
Flax	36	56
Hemp	42	53
Eucalyptus	41	59

[a] activation time = 50 min

Analysis of Pore Structure Determined by Gas Sorption

The sorptive properties of the lignin-derived chars and carbons were determined using low-pressure gas sorption analysis, up to 1 bar. Analysis of the lignin chars revealed the materials were non-porous to N_2 at -196 °C and exhibited a small CO_2 uptake of 10-15 $cm^3 \cdot g^{-1}$ at 0 °C (for the isotherms, see **Figure S3** in *Supplementary Information*), indicating chars have a limited porous network composed of ultramicropores (pores below 7 Å diameter) inaccessible to N_2. No influence of aromatic lignin structure was discernible on the uptake behavior of these low-temperature lignin chars.

The activation process enhances the rudimentary porosity of chars created in the pyrolysis stage. Consequently, any influence of the aromatic structure on lignin carbons should become apparent upon activation. N_2 isotherms for lignin-derived activated carbons recorded at -196 °C are shown in **Figure 2A**. Representative isotherms are shown here with tabulated data including duplicate runs listed in **Table S2** in the *Supplementary Information*. All activated carbons exhibit Type 1 behavior associated with microporous materials; adsorption chiefly occurs at low relative pressure ($p/p_0 < 0.1$), with little evidence of further adsorption in the meso- and macropore range ($p/p_0 \sim 0.1$-1.0). Adsorptive characteristics were derived from the N_2 isotherms (**Figure 2B**), including the maximum quantity of gas adsorbed (Max Q_{ads}), the total (V_{tot}) and micro- (V_{micro}) pore volumes, the BET (S_{BET}) and micropore (S_{micro}) surface area, and the volume-weighted average pore size (w_{avg}:2D-NLDFT). The results presented here show a comparable adsorptive performance across all lignin carbons, irrespective of aromatic structure.

Both the low-S/G and high-S/G lignin-derived carbons exhibit a similar BET surface area of 1064-1258 $m^2 \cdot g^{-1}$ (± <30 $m^2 \cdot g^{-1}$) and total pore volume of 0.42-0.52 $cm^3 \cdot g^{-1}$ (±≤0.03 $cm^3 \cdot g^{-1}$). **Figure 2C** shows all materials are highly microporous, with V_{micro} contributing 81-86 % to the total pore volume and S_{micro} contributing 81-89 % to the BET surface area indicating an absence of meso- and macroporosity.

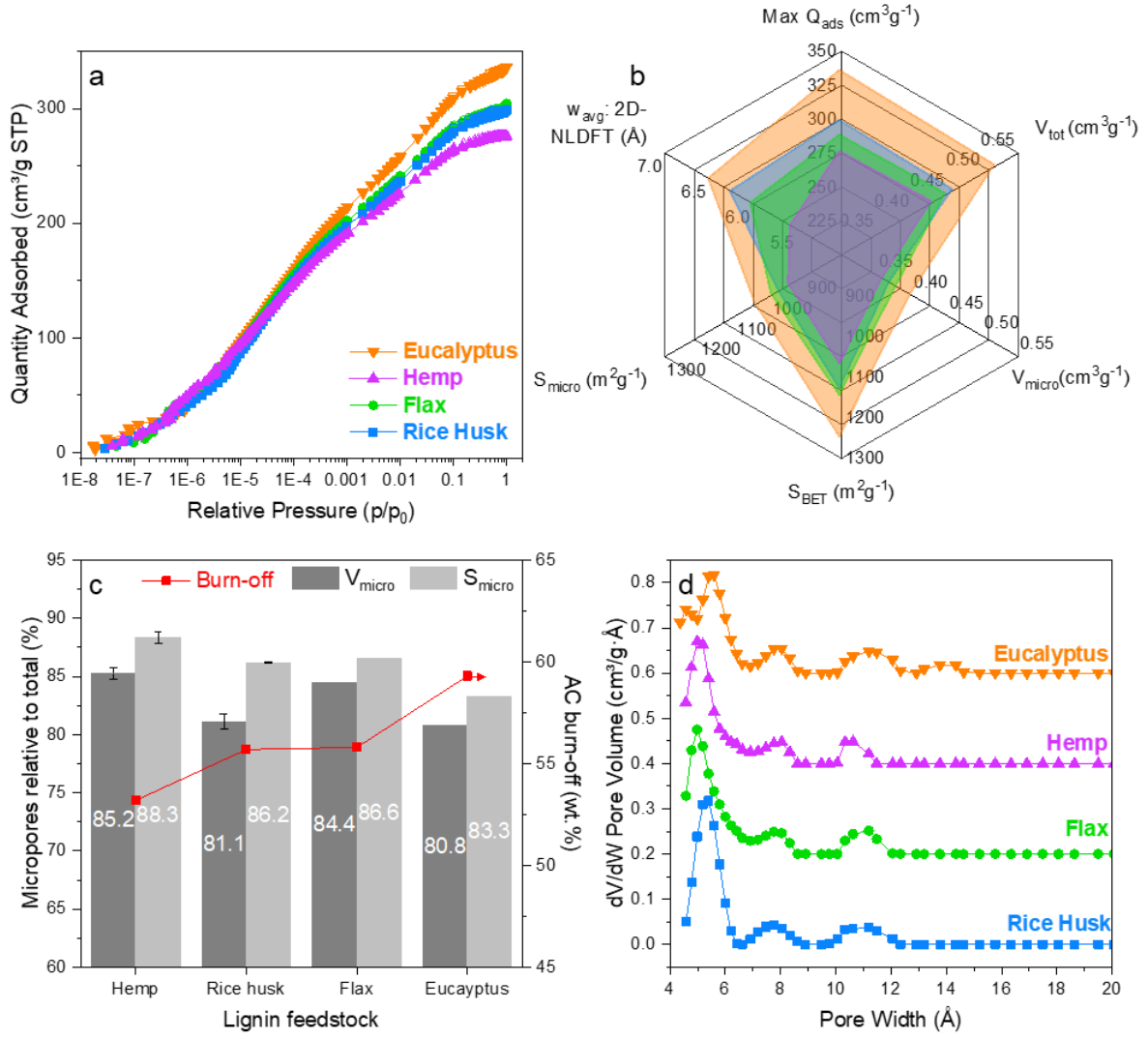

Figure 2. Adsorptive characterization of activated carbons derived from different types of organosolv lignin; flax, rice husk, hemp, and eucalyptus. (a) Nitrogen sorption isotherms at -196 °C up to 1 bar on a logarithmic scale, symbols are filed for the adsorption branch and empty for the desorption. (b) Comparison of adsorptive properties derived from nitrogen sorption isotherms; maximum quantity of gas adsorbed (Max Q_{ads}), the total (V_{tot}) and micro- (V_{micro}) pore volumes, the BET (S_{BET}) and micropore (S_{micro}) surface area, and volume-weighted average pore size by fitting of the 2D-NLDFT model to nitrogen sorption isotherms. Values are listed in **Table S2** in the *Supplementary Information*. (c) Comparison of V_{micro} and S_{micro} relative to V_{tot} and S_{BET}, and their relation to activated carbon (AC) burn-off. Duplicate isotherm measurements were performed for rice husk and hemp lignin carbons, with uncertainty values indicating the maximum deviation of measurements from the mean. (d) Differential pore volume pore size distributions calculated from the 2D-NLDFT model. Nitrogen isotherms on

a linear scale and the cumulative pore size distribution calculated from the 2D-NLDFT model are included in **Figure S4** in the *Supplementary Information*.

There are small variations evident within the adsorptive properties of lignin-derived activated carbons; however, these appear to correlate to minor differences in burn-off. The eucalyptus lignin carbon, with the highest burn-off (59 wt.%) exhibits the largest adsorptive property values. Conversely, the hemp lignin carbon with the lowest burn-off (53 wt.%) exhibits the smallest adsorptive property values. This is illustrated further in **Figure 2C**: the high S/G hemp lignin carbon has an increased contribution of microporosity to V_{tot} and S_{BET} (85 % and 81 %, respectively) than the eucalyptus lignin carbon (81 % and 83 % respectively). The increase in burn-off exhibited by the eucalyptus lignin-derived activated carbon results in a widening of microporosity.

Pore size distributions were extracted from the N_2 isotherms for a more detailed examination of the carbon porosity and are shown in **Figure 2D**. All lignin carbons exhibit a similar distribution with pores divided into groups of four different widths: below 7 Å, 7-9 Å, 9-20 Å, and above 20 Å. The contribution of these micropore groups to the total pore volume (listed in **Table 2**) is similar across all the activated carbons; the most significant contribution is from ultramicropores below 7 Å width (64-76 vol.%), with further significant contributions from larger micropores between 7 Å and 9 Å in width (~12 vol.%) and between 9 Å and 20 Å in width (9-20 vol.%). Mesopores above 20 Å in width have only a small contribution (<5 vol.%) to the total pore volume.

Table 2. Relative volume of micropores of specified pore width (*w*) to the total pore volume of lignin-derived activated carbons from different feedstocks. Micropore volumes were calculated from pore size distributions, derived by the fitting of the 2D-NLDFT model to nitrogen isotherms recorded at -196 °C up to 1 bar. Duplicate full isotherm measurements were performed for rice husk and hemp lignin carbons, with uncertainty values indicating the maximum deviation of measurements from the mean.

Lignin Feedstock	Pore Volume Contribution (vol.%)			
	w < 7 Å	7 Å ≤ w < 9 Å	9 Å≤ w < 20 Å	w > 20 Å
Hemp	76±1	12±<1	9±1	3±<1
Rice Husk	71±2	11±2	14±1	4±<1
Flax	70	12	14	4
Eucalyptus	64	11	20	5

The aromatic ratio of the lignin feedstock appears to have little effect on the micropore distribution. Akin to the adsorptive properties, small variations in the microporosity of lignin carbons can be attributed to differences in burn-off. The contribution from ultramicropores below 7 Å decreases with increasing burn-off from 76 wt.% for the hemp lignin carbon (53 wt.% burn-off), to about 70 wt.% for the flax and rice husk lignin carbons (55 wt.% burn-off), and 64 wt.% for the eucalyptus lignin carbon (59 wt.% burn-off). Conversely, the contribution to the total pore volume from larger micropores between 9 Å and 20 Å increases with increasing burn-off from 9 % for the hemp, to 14 % for the rice husk and flax, and 20 % for the eucalyptus. These results indicate that increasing burn-off causes a widening of ultramicropores with diameters below 7 Å. The widening of activated carbon pore size with increasing burn-off is a well-reported phenomenon throughout the literature.[55,57–61]

Effect on Activated Carbon Structure

Structural characterization with X-ray scattering indicates all lignin carbons exhibit a low degree of graphitization, from the absence of sharp reflections.[14,62,63] As seen from **Figure 3A**, there are two broad peaks in all activated carbon spectra at 2θ = 22° (d = 4.1 Å) and 2θ = 44° (d = 2.2 Å), characteristic of the (002) and (100/101) reflection of graphite, respectively.[64–66]

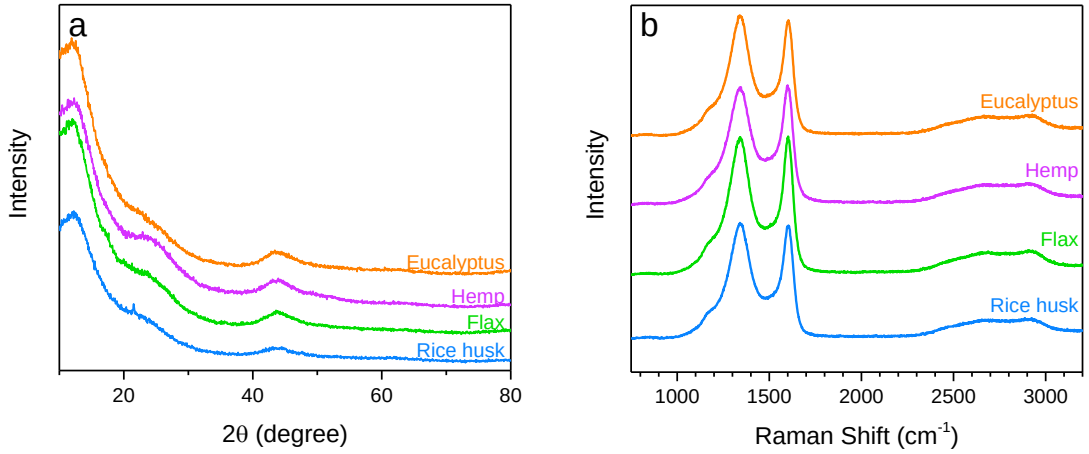

Figure 3. (a) X-ray diffraction patterns and (b) Raman spectra of activated carbons derived from different lignin feedstocks; eucalyptus, hemp, flax, and rice husk. For XRD patterns, removal of a background correction of silicon sample holder was performed, and spectra offset along the y-axis for clarity. For Raman spectra, a baseline correction was performed, and all spectra have been offset along the y-axis for clarity.

Raman spectra of all activated carbons (**Figure 3B**) show the presence of two broad peaks near 1340 cm^{-1} and 1600 cm^{-1}, which can be assigned to the D- and G-bands, respectively. These bands indicate the presence of both disordered (D) and graphitic sp^2 (G) carbon within the

materials. The broad D band, with an additional shoulder at 1155 cm^{-1}, corresponds with the XRD patterns, indicating all samples are primarily composed of amorphous carbon.

To further investigate the carbon structure, Raman spectra were deconvoluted into four peaks (see **Table 3** in the text and **Figure S5** in the *Supplementary Information)* attributed to the D1-, D2-, D3-, and G1-bands.[25,66–69] The G-band in all spectra is shifted away from single crystal graphite (at 1575 cm^{-1})[70] to higher values associated with nanocrystalline graphite (at 1600 cm^{-1}).[71] This shift indicates the presence of both an amorphous carbon phase and nanocrystalline domains within the lignin-derived activated carbons, supported by an I_D/I_G ratio of 2.5–2.9 (±0.8).[68,72] Such nanocrystalline domains, as remarked by Shimodaira & Masui,[72] are unlikely to have regular lattice structure like graphite but are likely to be composed of winding short basal planes.

XPS spectra (see **Figure S6** in the S*upplementary Information*) indicate the presence of carbon and oxygen in all activated carbons and the absence of other detectable elements.[73,74] Deconvolution of the C1s signal (see **Figure S7** in the *Supplementary Information*) supports the Raman results, indicating the presence of both sp^2 and sp^3 carbon in the samples.[75]

Table 3. Parameters obtained by deconvolution of Raman spectra by fitting of 4 peaks (D2, D1, D3, G1, D4) using the Voigt function. Spectra were recorded in triplicate; the mean values are reported here with uncertainty values representing the standard deviation across measurements.

Lignin Feedstock	Mode	Peak Position (cm^{-1})	FWHM (cm^{-1})	I_D/I_G
Rice Husk	D	1342±1	129±7	2.47±0.53
	G	1602±4	62±2	
Flax	D	1343±2	136±12	2.93±0.61
	G	1605±1	63±4	
Hemp	D	1346±4	132±8	2.75±0.79
	G	1605±3	62±4	
Eucalyptus	D	1343±2	124±4	2.81±0.85
	G	1605±1	62±3	

Effect of Aromatic Structure on the Hydrogen Uptake

Table 4. Gravimetric hydrogen uptake of TE7 beads and lignin activated carbons (LACs) derived from different biomass feedstocks: rice husk (R), flax (F), hemp (H), and eucalyptus (E). Hydrogen isotherms were recorded in triplicate; the mean values are reported here with uncertainty values representing the standard deviation across measurements.

Activated Carbon	Gravimetric H_2 Uptake (wt.%)
RLAC	1.6±0.1
FLAC	1.7±0.1
HLAC	1.5±0.1
ELAC	1.8±0.2
TE7	2.0±0.1

The consistency of lignin-derived activated carbon performance was evaluated by determination of the gravimetric hydrogen storage capacity at -196 °C up to 1 bar. Hydrogen isotherms are shown in **Figure 4** with gravimetric uptake values listed in **Table 4**. For comparison, a well-characterized and industrially produced activated carbon, TE7,[8,76,77] was examined. TE7 carbons beads are produced from phenolic resin and have a similar BET surface area (1400 $m^2 \cdot g^{-1}$ see **Figure S8** in the S*upplementary Information*) to the lignin carbons in this work. There is no hysteresis between the adsorption and desorption branches of the Type 1 isotherms, indicating hydrogen adsorption was completely reversible across all carbon materials. The lignin carbons show similar uptake values of 1.5 to 1.8 wt.%. TE7 exhibited an uptake of 2.0 wt.%, comparable to values reported previously for this material.[77] The lignin-derived carbons in this work exhibit comparable hydrogen uptake capacity to carbide-derived carbons (1.2 wt.% to 3.0 wt.%)[78,79] with the advantage of a facile synthesis method and a cheap and widely available starting feedstock. The lignin carbons also show similar hydrogen uptake values to other physically activated biomass-derived carbons[73,80–82] with a similar specific surface area (1.3 wt.% to 2.5 wt.%).

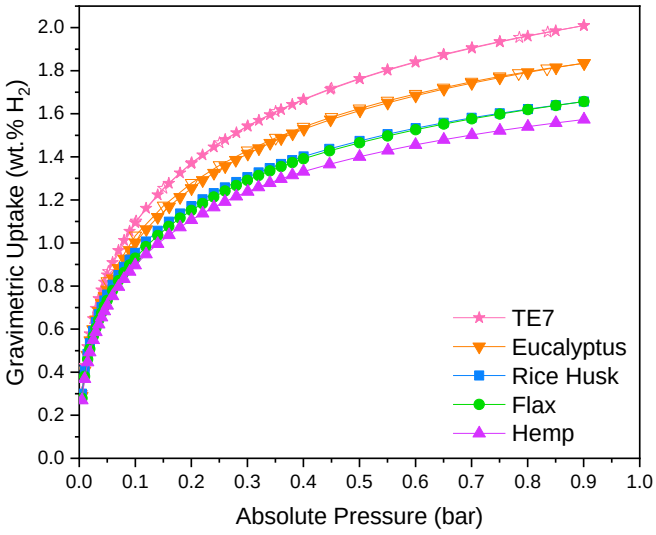

Figure 4. Hydrogen sorption isotherms showing gravimetric uptake at -196 °C in activated carbons derived from different types of lignin: eucalyptus, hemp, flax, and rice husk. An industrially produced activated carbon, TE7, is included for comparison. Symbols are filled for the adsorption branch and empty for the desorption branch.

Small differences in the hydrogen capacity of lignin-derived carbons are evident. The uptake of the hemp and eucalyptus-derived samples appear to be slightly lower and higher, respectively, reflecting the differences in micropore surface area and micropore volume resulting from small variations in sample burn-off. Isotherms normalized to the maximum uptake of hydrogen (see **Figure S9** in the *Supplementary Information*) show little variation across the four different lignin-derived carbons, indicating a comparable interaction between the H_2 molecules and pores in all samples. The nitrogen sorption results indicate this similarity can be attributed to the comparable pore size distributions of all lignin-derived activated carbons, and equivalent contribution of micropores associated with hydrogen uptake (below 7 Å) to the total pore volume across all samples (81 to 86 wt.%).

The hydrogen capacity results presented here support the findings of the characterization section: porosity of the lignin-derived carbon powders is almost identical and, therefore, can be decoupled from the initial differences in the aromatic lignin structure. The gas sorption results in this work indicate the successful production of activated carbons with consistent adsorptive properties, independent of the aromatic lignin structure, by employing a low temperature carbonization with a short dwell time.

S-unit rich lignins are expected to produce activated carbons with increased adsorptive properties in comparison to G-unit rich lignin chars, due to differences in their thermal behavior. Lignin is generally accepted to undergo pyrolysis via a free-radical mechanism.[23,83–85] The loss of low molecular weight volatiles during pyrolysis leads to the formation of a rudimentary

porous structure in the char.[25] The additional methoxy group in S-units leads to the increased formation of methoxyl radicals during pyrolysis, which is believed to stabilize large molecular fragments, preventing char formation and promoting volatile evolution.[83,86] Increased devolatilisation of lignin chars rich in S-units is demonstrated in this work, and in the literature, by lower char yields during thermogravimetric analysis.[24,83,86] Increased devolatilization can lead to an increased char surface area, which in turn, can cause an increased rate of activation due to a larger quantity of active sites for CO_2 adsorption. [19,20,87,88]

The carbonization process in this work utilized a low temperature and limited dwell time, inhibiting the release of low molecular weight volatiles, and consequently, the rudimentary porosity formed in the char. Chars prepared from both S-unit rich lignin and G-unit rich lignin, therefore, exhibited a similar, limited porous structure, as demonstrated by their low CO_2 uptake and non-porous nature to N_2. Activation enhances the rudimentary porosity within the original char. Without differences in porosity at the char stage, the subsequent activation proceeded in a similar manner for both sets of lignin chars.

Lignin-derived activated carbons from both low S/G ratio lignin and high S/G ratio lignin exhibited comparable adsorptive properties and hydrogen uptake capacities, with minor variations between materials due to small differences in burn-off. It should be noted that, as in the case of rice husk lignin, the burn-off rate for activated carbons can be affected by impurities in the feedstock. However, this does not appear to affect activated carbon porosity. The activation time should be adjusted accordingly to the appropriate level of burn-off. These findings have important implications for the industrial scale-up of the lignin-derived activated carbon production. By utilizing a low carbonization temperature and short dwell time in lignin carbon synthesis, activated carbon materials with consistent adsorptive properties and hydrogen capacity can be produced from different lignin biomass sources. Consequently, the manufacturing process is not reliant on lignin from one biomass source and would be resistant to changes in the changes in the supply chain, such as seasonal variations in the lignin feedstock.

Conclusions

Our findings showed that by carefully controlling the pyrolysis conditions, the effect of the aromatic ratio of the lignin on the adsorptive properties and hydrogen uptake capacity of resulting lignin-derived activated carbon materials can be negated. Small deviations between adsorptive properties and hydrogen capacity can be attributed to small differences in material burn-off, causing variations in the micropore distribution. The use of a low carbonization temperature means the process is resilient to variations in the organosolv lignin material, which

could be caused by a change in biomass source or growing conditions. Thus, any organosolv lignin can be utilized as a feedstock to produce a reliable, high surface area (> 1000 m^2 g^{-1}) activated carbon product with consistent adsorptive performance. An additional benefit is that the relatively low pyrolysis temperatures used will incur less of an energy penalty for industrial processes, making large scale production more efficient. The lignin-derived carbons in this work exhibited hydrogen uptake values of up to 1.8 wt.% comparable to other activated carbon materials, reinforcing the idea that carbon-based materials resulting from waste lignin may be an economical and sustainable option for future large-scale hydrogen storage applications.

Supporting Information

- NMR spectra, full purity and molecular weight analysis for the extracted lignins, photographs of lignin chars, Raman spectra and XPS spectra of lignin activated carbons, and gas sorption isotherms for all carbon materials. The Supporting Information is available online free of charge at https://pubs.acs.org/.

Acknowledgements

The authors thank Steve Tennison at CarbonTex Ltd (formerly MAST Carbon) for supplying the four biomass feedstocks used in this work, Tim Woodman at the University of Bath for his support acquiring the 2D-NMR spectra, Natalie Pridmore at the University of Bristol for her assistance collecting XRD patterns of the lignin carbons. The authors acknowledge the Bristol NanoESCA Facility (EPSRC Strategic Equipment Grant EP/K035746/1 and EP/M000605/1) for the collection of XPS spectra. VPT thanks the Engineering and Physical Sciences Research Council (EPSRC) for support via EP/R01650X/1. All relevant raw data is included in the manuscript or the electronic supplementary information.

Bibliography

(1) Sevilla, M.; Mokaya, R. Energy Storage Applications of Activated Carbons: Supercapacitors and Hydrogen Storage. *Energy Environ. Sci.* **2014**, *7* (4), 1250–1280. https://doi.org/10.1039/C3EE43525C.

(2) Yu, X.; Tang, Z.; Sun, D.; Ouyang, L.; Zhu, M. Recent Advances and Remaining Challenges of Nanostructured Materials for Hydrogen Storage Applications. *Prog. Mater. Sci.* **2017**, *88*, 1–48. https://doi.org/10.1016/j.pmatsci.2017.03.001.

(3) Xia, Y.; Yang, Z.; Zhu, Y. Porous Carbon-Based Materials for Hydrogen Storage: Advancement and Challenges. *J. Mater. Chem. A* **2013**, *1* (33), 9365–9381. https://doi.org/10.1039/c3ta10583k.

(4) Masika, E.; Mokaya, R. Hydrogen Storage in High Surface Area Carbons with Identical Surface Areas but Different Pore Sizes: Direct Demonstration of the Effects of Pore Size. *J. Phys. Chem. C* **2012**, *116* (49), 25734–25740. https://doi.org/10.1021/jp3100365.

(5) Gogotsi, Y.; Dash, R. K.; Yushin, G.; Yildirim, T.; Laudisio, G.; Fischer, J. E. Tailoring of Nanoscale Porosity in Carbide-Derived Carbons for Hydrogen Storage. *J. Am. Chem. Soc.* **2005**, *127* (46), 16006–16007. https://doi.org/10.1021/ja0550529.

(6) Gogotsi, Y.; Portet, C.; Osswald, S.; Simmons, J. M.; Yildirim, T.; Laudisio, G.; Fischer, J. E. Importance of Pore Size in High-Pressure Hydrogen Storage by Porous Carbons. *Int. J. Hydrogen Energy* **2009**, *34* (15), 6314–6319. https://doi.org/10.1016/j.ijhydene.2009.05.073.

(7) Sethia, G.; Sayari, A. Activated Carbon with Optimum Pore Size Distribution for Hydrogen Storage. *Carbon N. Y.* **2016**, *99*, 289–294. https://doi.org/10.1016/j.carbon.2015.12.032.

(8) Ting, V. P.; Ramirez-Cuesta, A. J.; Bimbo, N.; Sharpe, J. E.; Noguera-Diaz, A.; Presser, V.; Rudic, S.; Mays, T. J. Direct Evidence for Solid-like Hydrogen in a Nanoporous Carbon Hydrogen Storage Material at Supercritical Temperatures. *ACS Nano* **2015**, *9* (8), 8249–8254. https://doi.org/10.1021/acsnano.5b02623.

(9) Carrott, P.; Carrott, M. R. Lignin, from Natural Adsorbent to Activated Carbon: A Review. *Bioresour. Technol.* **2007**, *98* (12), 2301–2312. https://doi.org/10.1016/j.biortech.2006.08.008.

(10) Souto, F.; Calado, V.; Pereira, N. Lignin-Based Carbon Fiber: A Current Overview. *Mater. Res. Express* **2018**, *5* (7), 072001. https://doi.org/10.1088/2053-1591/aaba00.

(11) Calvo-Flores, F. G.; Dobado, J. A. Lignin as Renewable Raw Material. *ChemSusChem* **2010**, *3* (11), 1227–1235. https://doi.org/10.1002/cssc.201000157.

(12) Rowlandson, J. L.; OBrien, J. C.; Edler, K. J.; Tian, M.; Ting, V. P. Application of Experimental Design to Hydrogen Storage: Optimisation of Lignin-Derived Carbons. *J. Carbon Res.* **2019**, *5* (4), 82. https://doi.org/10.3390/C5040082.

(13) Sumathi, S.; Bhatia, S.; Lee, K. T.; Mohamed, A. R. Optimization of Microporous Palm Shell Activated Carbon Production for Flue Gas Desulphurization: Experimental and Statistical Studies. *Bioresour. Technol.* **2009**, *100* (4), 1614–1621. https://doi.org/10.1016/j.biortech.2008.09.020.

(14) Loloie, Z.; Mozaffarian, M.; Soleimani, M.; Asassian, N. Carbonization and CO2

Activation of Scrap Tires: Optimization of Specific Surface Area by the Taguchi Method. *Korean J. Chem. Eng.* **2017**, *34* (2), 366–375. https://doi.org/10.1007/s11814-016-0266-4.

(15) Baçaoui, A.; Dahbi, A.; Yaacoubi, A.; Bennouna, C.; Maldonado-Hódar, F.; Rivera-Utrilla, J.; Carrasco-Marín, F.; Moreno-Castilla, C. Experimental Design To Optimize Preparation of Activated Carbons for Use in Water Treatment. *Environ. Sci. Technol.* **2002**, *36* (17) 3844-3849. https://doi.org/10.1021/ES010305T.

(16) Zhao, W.; Fierro, V.; Zlotea, C.; Aylon, E.; Izquierdo, M. T.; Latroche, M.; Celzard, A. Optimization of Activated Carbons for Hydrogen Storage. *Int. J. Hydrogen Energy* **2011**, *36* (18), 11746–11751. https://doi.org/10.1016/j.ijhydene.2011.05.181.

(17) Mussatto, S.; Fernandes, M.; Rocha, G. Production, Characterization and Application of Activated Carbon from Brewer's Spent Grain Lignin. *Bioresour. Technol* **2010**, *101*, 2450–2457.

(18) Sangchoom, W.; Mokaya, R. Valorization of Lignin Waste: Carbons from Hydrothermal Carbonization of Renewable Lignin as Superior Sorbents for CO2 and Hydrogen Storage. *ACS Sustain. Chem. Eng.* **2015**, *3* (7), 1658–1667. https://doi.org/10.1021/acssuschemeng.5b00351.

(19) Adschiri, T.; Furusawa, T. Relation between CO2-Reactivity of Coal Char and BET Surface Area. *Fuel* **1986**, *65* (7), 927–931. https://doi.org/10.1016/0016-2361(86)90200-0.

(20) Cetin, E.; Moghtaderi, B.; Gupta, R.; Wall, T. F. Influence of Pyrolysis Conditions on the Structure and Gasification Reactivity of Biomass Chars. *Fuel* **2004**, *83* (16), 2139–2150. https://doi.org/10.1016/j.fuel.2004.05.008.

(21) Sun, Q.; Khunsupat, R.; Akato, K.; Tao, J.; Labbé, N.; Gallego, N. C.; Bozell, J. J.; Rials, T. G.; Tuskan, G. A.; Tschaplinski, T. J.; et al. A Study of Poplar Organosolv Lignin after Melt Rheology Treatment as Carbon Fiber Precursors. *Green Chem.* **2016**, *18* (18), 5015–5024. https://doi.org/10.1039/c6gc00977h.

(22) Gao, Y.; Li, L.; Jin, Y.; Wang, Y.; Yuan, C.; Wei, Y.; Chen, G.; Ge, J.; Lu, H. Porous Carbon Made from Rice Husk as Electrode Material for Electrochemical Double Layer Capacitor. *Appl. Energy* **2015**, *153*, 41–47. https://doi.org/10.1016/j.apenergy.2014.12.070.

(23) Bährle, C.; Custodis, V.; Jeschke, G.; Van Bokhoven, J. A.; Vogel, F. In Situ Observation of Radicals and Molecular Products during Lignin Pyrolysis. *ChemSusChem* **2014**, *7* (7), 2022–2029. https://doi.org/10.1002/cssc.201400079.

(24) Rowlandson, J. L.; Woodman, T. J.; Tennison, S. R.; Edler, K. J.; P. Ting, V. Influence of Aromatic Structure on the Thermal Behaviour of Lignin. *Waste and Biomass Valorization* **2018**, 1–14. https://doi.org/10.1007/s12649-018-0537-x.

(25) Jeon, J.-W.; Zhang, L.; Lutkenhaus, J. L.; Laskar, D. D.; Lemmon, J. P.; Choi, D.; Nandasiri, M. I.; Hashmi, A.; Xu, J.; Motkuri, R. K.; et al. Controlling Porosity in Lignin-Derived Nanoporous Carbon for Supercapacitor Applications. *ChemSusChem* **2014**, *8* (3), 428–432. https://doi.org/10.1002/cssc.201402621.

(26) Carrott, P. J. M.; Suhas; Carrott, M. M. L. R.; Guerrero, C. I.; Delgado, L. A. Reactivity and Porosity Development during Pyrolysis and Physical Activation in CO2 or Steam of Kraft and Hydrolytic Lignins. *J. Anal. Appl. Pyrolysis* **2008**, *82* (2), 264–

271. https://doi.org/10.1016/j.jaap.2008.04.004.

(27) U.S Deparment of Energy. DOE Technical Targets for Onboard Hydrogen Storage for Light-Duty Vehicles https://www.energy.gov/eere/fuelcells/doe-technical-targets-onboard-hydrogen-storage-light-duty-vehicles (accessed Aug 28, 2019).

(28) SMMT. Car Registrations https://www.smmt.co.uk/vehicle-data/car-registrations/ (accessed Aug 23, 2019).

(29) Marsh, H.; Rodríguez-Reinoso, F. *Activated Carbon*; Elsevier, 2006. https://doi.org/10.1016/B978-008044463-5/50013-3.

(30) Pye, E. K.; Lora, J. H. The AlcellTM Process : A Proven Alternative to Kraft Pulping. *Tappi J.* **1991**, *74* (3), 113–118.

(31) Botello, J. I.; Gilarranz, M. A.; Rodriguez, F.; Oliet, M. Recovery of Solvent and By-Products from Organosolv Black Liquor. *Sep. Sci. Technol.* **1999**, *34* (12), 2431–2445. https://doi.org/10.1081/SS-100100783.

(32) Gandolfi, S.; Ottolina, G.; Consonni, R.; Riva, S.; Patel, I. Fractionation of Hemp Hurds by Organosolv Pretreatment and Its Effect on Production of Lignin and Sugars. *ChemSusChem* **2014**, *7* (7), 1991–1999. https://doi.org/10.1002/cssc.201301396.

(33) Lora, J. H.; Katzen, R.; Cronlund, M.; Wu, C. F. Recovery of Lignin. US4764596, August 16, 1988.

(34) Celignis Limited. Celignis Analytical http://www.celignis.com/ (accessed Dec 12, 2017).

(35) Constant, S.; Wienk, H. L. J.; Frissen, A. E.; Peinder, P. de; Boelens, R.; Es, D. S. van; Grisel, R. J. H.; Weckhuysen, B. M.; Huijgen, W. J. J.; Gosselink, R. J. A.; et al. New Insights into the Structure and Composition of Technical Lignins: A Comparative Characterisation Study. *Green Chem.* **2016**, *18* (9), 4888–4907. https://doi.org/10.1039/C5GC03043A.

(36) Gosselink, R. J. A.; Abächerli, A.; Semke, H.; Malherbe, R.; Käuper, P.; Nadif, A.; van Dam, J. E. G. Analytical Protocols for Characterisation of Sulphur-Free Lignin. *Ind. Crops Prod.* **2004**, *19* (3), 271–281. https://doi.org/10.1016/j.indcrop.2003.10.008.

(37) del Río, J. C.; Rencoret, J.; Marques, G.; Gutiérrez, A.; Ibarra, D.; Santos, J. I.; Jiménez-Barbero, J.; Zhang, L.; Martínez, A. T. Highly Acylated (Acetylated and/or p-Coumaroylated) Native Lignins from Diverse Herbaceous Plants. *J. Agric. Food Chem.* **2008**, *56* (20), 9525–9534. https://doi.org/10.1021/jf800806h.

(38) Wen, J. L.; Sun, S. L.; Yuan, T. Q.; Xu, F.; Sun, R. C. Structural Elucidation of Lignin Polymers of Eucalyptus Chips during Organosolv Pretreatment and Extended Delignification. *J. Agric. Food Chem.* **2013**, *61* (46), 11067–11075. https://doi.org/10.1021/jf403717q.

(39) Salanti, A.; Zoia, L.; Orlandi, M.; Zanini, F.; Elegir, G. Structural Characterization and Antioxidant Activity Evaluation of Lignins from Rice Husk. *J. Agric. Food Chem.* **2010**, *58* (18), 10049–10055. https://doi.org/10.1021/jf102188k.

(40) Yuan, T.-Q.; Sun, S.-N.; Xu, F.; Sun, R.-C. Characterization of Lignin Structures and Lignin-Carbohydrate Complex (LCC) Linkages by Quantitative 13C and 2D HSQC NMR Spectroscopy. *J. Agric. Food Chem.* **2011**, *59* (19), 10604–10614. https://doi.org/10.1021/jf2031549.

(41) Hjaila, K.; Baccar, R.; Sarrà, M.; Gasol, C. M.; Blánquez, P. Environmental Impact Associated with Activated Carbon Preparation from Olive-Waste Cake via Life Cycle Assessment. *J. Environ. Manage.* **2013**, *130*, 242–247. https://doi.org/10.1016/j.jenvman.2013.08.061.

(42) Arena, N.; Lee, J.; Clift, R. Life Cycle Assessment of Activated Carbon Production from Coconut Shells. *J. Clean. Prod.* **2016**, *125*, 68–77. https://doi.org/10.1016/j.jclepro.2016.03.073.

(43) ISO. Pore Size Distribution and Porosity of Solid Materials by Mercury Porosimetry and Gas Adsorption -- Part 3: Analysis of Micropores by Gas Adsorption. *ISO 15901-3* **2007**, 1–27.

(44) ISO. Determination of the Specific Surface Area of Solids by Gas Adsorption. BET Method. *ISO 9277* **2010**, 1–24. https://doi.org/10.3403/30180119.

(45) Laudisio, G.; Dash, R. K.; Singer, J. P.; Yushin, G.; Gogotsi, Y.; Fischer, J. E. Carbide-Derived Carbons: A Comparative Study of Porosity Based on Small-Angle Scattering and Adsorption Isotherms. *Langmuir* **2006**, *22* (21), 8945–8950. https://doi.org/10.1021/LA060860E.

(46) Hiden Isochema. Hydrogen Storage Capacity of Materials https://www.azom.com/article.aspx?ArticleID=12464#2 (accessed Jul 16, 2018).

(47) Monteil-Rivera, F.; Phuong, M.; Ye, M.; Halasz, A.; Hawari, J. Isolation and Characterization of Herbaceous Lignins for Applications in Biomaterials. *Ind. Crops Prod.* **2013**, *41*, 356–364. https://doi.org/10.1016/j.indcrop.2012.04.049.

(48) Tejado, A.; Peña, C.; Labidi, J.; Echeverria, J. M.; Mondragon, I. Physico-Chemical Characterization of Lignins from Different Sources for Use in Phenol-Formaldehyde Resin Synthesis. *Bioresour. Technol.* **2007**, *98* (8), 1655–1663. https://doi.org/10.1016/j.biortech.2006.05.042.

(49) Chen, C.-L. Nitrobenzene and Cupric Oxide Oxidations. In *Methods in lignin chemistry*; Lin, S. Y., Dence, C. W., Eds.; Springer: Berlin, Heidelberg, 1992; pp 301–321.

(50) Del Río, J. C.; Rencoret, J.; Prinsen, P.; Martínez, Á. T.; Ralph, J.; Gutiérrez, A. Structural Characterization of Wheat Straw Lignin as Revealed by Analytical Pyrolysis, 2D-NMR, and Reductive Cleavage Methods. *J. Agric. Food Chem.* **2012**, *60* (23), 5922–5935. https://doi.org/10.1021/jf301002n.

(51) Lua, A. C.; Yang, T.; Guo, J. Effects of Pyrolysis Conditions on the Properties of Activated Carbons Prepared from Pistachio-Nut Shells. *J. Anal. Appl. Pyrolysis* **2004**, *72* (2), 279–287. https://doi.org/10.1016/j.jaap.2004.08.001.

(52) Lua, A. C.; Lau, F. Y.; Guo, J. Influence of Pyrolysis Conditions on Pore Development of Oil-Palm-Shell Activated Carbons. *J. Anal. Appl. Pyrolysis* **2006**, *76* (1–2), 96–102. https://doi.org/10.1016/j.jaap.2005.08.001.

(53) Guo, J.; Chong Lua, A. Characterization of Chars Pyrolyzed from Oil Palm Stones for the Preparation of Activated Carbons. *J. Anal. Appl. Pyrolysis* **1998**, *46* (2), 113–125. https://doi.org/10.1016/S0165-2370(98)00074-6.

(54) Jia, Q.; Lua, A. C. Effects of Pyrolysis Conditions on the Physical Characteristics of Oil-Palm-Shell Activated Carbons Used in Aqueous Phase Phenol Adsorption. *J. Anal. Appl. Pyrolysis* **2008**, *83* (2), 175–179. https://doi.org/10.1016/j.jaap.2008.08.001.

(55) Bansal, R. C.; Donet, J. B.; Stoeckli, H. F. *Active Carbon*; M. Dekker: New York, 1988.

(56) Mohamad Nor, N.; Lau, L. C.; Lee, K. T.; Mohamed, A. R. Synthesis of Activated Carbon from Lignocellulosic Biomass and Its Applications in Air Pollution Control—a Review. *J. Environ. Chem. Eng.* **2013**, *1* (4), 658–666. https://doi.org/10.1016/j.jece.2013.09.017.

(57) Daud, W. M. A. W.; Ali, W. S. W. Comparison on Pore Development of Activated Carbon Produced from Palm Shell and Coconut Shell. *Bioresour. Technol.* **2004**, *93*, 63–69. https://doi.org/10.1016/j.biortech.2003.09.015.

(58) Chang, C.; Chang, C.; Tsai, W. Effects of Burn-off and Activation Temperature on Preparation of Activated Carbon from Corn Cob Agrowaste by CO(2) and Steam. *J. Colloid Interface Sci.* **2000**, *232* (1), 45–49. https://doi.org/10.1006/jcis.2000.7171.

(59) Dubinin, M. M.; Zaverina, E. D.; Timofeeva, D. P. Sorbtsiya I Struktura Aktivnykh Uglei. 6. Strukturnye Tipy Aktivnykh Uglei. *Zhurnal Fiz. Khimii* **1949**, *23* (10), 1129–1140.

(60) Guo, S.; Peng, J.; Li, W.; Yang, K.; Zhang, L.; Zhang, S.; Xia, H. Effects of CO2 Activation on Porous Structures of Coconut Shell-Based Activated Carbons. *Appl. Surf. Sci.* **2009**, *255* (20), 8443–8449. https://doi.org/10.1016/j.apsusc.2009.05.150.

(61) Rodríguez-Reinoso, F.; Molina-Sabio, M.; González, M. T. The Use of Steam and CO2 as Activating Agents in the Preparation of Activated Carbons. *Carbon N. Y.* **1995**, *33* (1), 15–23. https://doi.org/10.1016/0008-6223(94)00100-E.

(62) Dash, R.; Chmiola, J.; Yushin, G.; Gogotsi, Y.; Laudisio, G.; Singer, J.; Fischer, J.; Kucheyev, S. Titanium Carbide Derived Nanoporous Carbon for Energy-Related Applications. *Carbon N. Y.* **2006**, *44* (12), 2489–2497. https://doi.org/10.1016/j.carbon.2006.04.035.

(63) Qie, L.; Chen, W.; Xu, H.; Xiong, X.; Jiang, Y.; Zou, F.; Hu, X.; Xin, Y.; Zhang, Z.; Huang, Y. Synthesis of Functionalized 3D Hierarchical Porous Carbon for High-Performance Supercapacitors. *Energy Environ. Sci.* **2013**, *6*, 2497–2504. https://doi.org/10.1039/c3ee41638k.

(64) Zhang, W.; Lin, H.; Lin, Z.; Yin, J.; Lu, H.; Liu, D.; Zhao, M. 3 D Hierarchical Porous Carbon for Supercapacitors Prepared from Lignin through a Facile Template-Free Method. *ChemSusChem* **2015**, *8* (12), 2114–2122. https://doi.org/10.1002/cssc.201403486.

(65) Kennedy, L. J.; Vijaya, J. J.; Sekaran, G. Effect of Two-Stage Process on the Preparation and Characterization of Porous Carbon Composite from Rice Husk by Phosphoric Acid Activation. *Ind. Eng. Chem. Res.* **2004**, *43* (8), 1832–1838. https://doi.org/10.1021/ie034093f.

(66) Bratek, W.; Świątkowski, A.; Pakuła, M.; Biniak, S.; Bystrzejewski, M.; Szmigielski, R. Characteristics of Activated Carbon Prepared from Waste PET by Carbon Dioxide Activation. *J. Anal. Appl. Pyrolysis* **2013**, *100*, 192–198. https://doi.org/10.1016/j.jaap.2012.12.021.

(67) Jeon, J.-W.; Sharma, R.; Meduri, P.; Arey, B. W.; Schaef, H. T.; Lutkenhaus, J. L.; Lemmon, J. P.; Thallapally, P. K.; Nandasiri, M. I.; McGrail, B. P.; et al. In Situ One-Step Synthesis of Hierarchical Nitrogen-Doped Porous Carbon for High-Performance

Supercapacitors. *ACS Appl. Mater. Interfaces* **2014**, *6* (10), 7214–7222. https://doi.org/10.1021/am500339x.

(68) Macedo, J. S.; Otubo, L.; Ferreira, O. P.; Gimenez, I. de F.; Mazali, I. O.; Barreto, L. S. Biomorphic Activated Porous Carbons with Complex Microstructures from Lignocellulosic Residues. *Microporous Mesoporous Mater.* **2008**, *107* (3), 276–285. https://doi.org/10.1016/j.micromeso.2007.03.020.

(69) Bonso, J. S.; Kalaw, G. D.; Ferraris, J. P. High Surface Area Carbon Nanofibers Derived from Electrospun PIM-1 for Energy Storage Applications. *J. Mater. Chem. A* **2014**, *2* (2), 418–424. https://doi.org/10.1039/C3TA13779A.

(70) Tuinstra, F.; Koenig, J. L. Raman Spectrum of Graphite. *J. Chem. Phys.* **1970**, *53* (3), 1126–1130. https://doi.org/10.1063/1.1674108.

(71) Ferrari, A. C. Determination of Bonding in Diamond-like Carbon by Raman Spectroscopy. *Diam. Relat. Mater.* **2002**, *11* (3–6), 1053–1061. https://doi.org/10.1016/S0925-9635(01)00730-0.

(72) Shimodaira, N.; Masui, A. Raman Spectroscopic Investigations of Activated Carbon Materials. *J. Appl. Phys.* **2002**, *92* (2), 902–909. https://doi.org/10.1063/1.1487434.

(73) Li, Y.; Li, D.; Rao, Y.; Zhao, X.; Wu, M. Superior CO2, CH4, and H2 Uptakes over Ultrahigh-Surface-Area Carbon Spheres Prepared from Sustainable Biomass-Derived Char by CO2activation. *Carbon N. Y.* **2016**, *105*, 454–462. https://doi.org/10.1016/j.carbon.2016.04.036.

(74) Lei, Z.; Christov, N.; Zhang, L. L.; Zhao, X. S. Mesoporous Carbon Nanospheres with an Excellent Electrocapacitive Performance. *J. Mater. Chem.* **2011**, *21* (7), 2274–2281. https://doi.org/10.1039/C0JM03322G.

(75) Cheng, F.; Liang, J.; Zhao, J.; Tao, Z.; Chen, J. Biomass Waste-Derived Microporous Carbons with Controlled Texture and Enhanced Hydrogen Uptake. *Chem. Mater.* **2008**, *20* (5), 1889–1895. https://doi.org/10.1021/cm702816x.

(76) Bimbo, N.; Ting, V. P.; Sharpe, J. E.; Mays, T. J. Analysis of Optimal Conditions for Adsorptive Hydrogen Storage in Microporous Solids. *Colloids Surfaces A Physicochem. Eng. Asp.* **2013**, *437*, 113–119. https://doi.org/10.1016/j.colsurfa.2012.11.008.

(77) Hruzewicz-Kołodziejczyk, A.; Ting, V. P.; Bimbo, N.; Mays, T. J. Improving Comparability of Hydrogen Storage Capacities of Nanoporous Materials. *Int. J. Hydrogen Energy* **2012**, *37* (3), 2728–2736. https://doi.org/10.1016/j.ijhydene.2011.03.001.

(78) Wang, Z.; Sun, L.; Xu, F.; Zhou, H.; Peng, X.; Sun, D.; Wang, J.; Du, Y. Nitrogen-Doped Porous Carbons with High Performance for Hydrogen Storage. *Int. J. Hydrogen Energy* **2016**, *41* (20), 8489–8497. https://doi.org/10.1016/j.ijhydene.2016.03.023.

(79) Yushin, G.; Dash, R.; Jagiello, J.; Fischer, J. E.; Gogotsi, Y. Carbide-Derived Carbons: Effect of Pore Size on Hydrogen Uptake and Heat of Adsorption. *Adv. Funct. Mater.* **2006**, *16* (17), 2288–2293. https://doi.org/10.1002/adfm.200500830.

(80) Jang, H. S.; Mun, J.; Hong, W. G.; Lee, S. M.; Jeon, J. W.; Lee, C. Y.; Kim, H. J.; Kim, B. H. The Performance of Green Carbon as a Backbone for Hydrogen Storage Materials. *Int. J. Hydrogen Energy* **2019**. https://doi.org/10.1016/j.ijhydene.2019.03.084.

(81) Wang, H.; Gao, Q.; Hu, J. High Hydrogen Storage Capacity of Porous Carbons Prepared by Using Activated Carbon. *J. Am. Chem. Soc.* **2009**, *131* (20), 7016–7022. https://doi.org/10.1021/ja8083225.

(82) Bader, N.; Abdelmottaleb, O. CO2 Activation of Olive Bagasse for Hydrogen Storage. *Environ. Prog. Sustain. Energy* **2017**, *36* (1), 315–324. https://doi.org/10.1002/ep.12514.

(83) Jakab, E.; Faix, O.; Till, F. Thermal Decomposition of Milled Wood Lignins Studied by Thermogravimetry/Mass Spectrometry. *J. Anal. Appl. Pyrolysis* **1997**, *40–41*, 171–186. https://doi.org/10.1016/S0165-2370(97)00046-6.

(84) Avni, E.; Suib, S. L.; Coughlin, R. W. Free Radical Formation in Lignin During Pyrolysis. *Holzforsch. - Int. J. Biol. Chem. Phys. Technol. Wood* **1985**, *39*, 33–40. https://doi.org/10.1515/hfsg.1985.39.1.33.

(85) Kibet, J.; Khachatryan, L.; Dellinger, B. Molecular Products and Radicals from Pyrolysis of Lignin. *Environ. Sci. Technol.* **2012**, *46* (23), 12994–13001. https://doi.org/10.1021/es302942c.

(86) Wang, S.; Ru, B.; Lin, H.; Sun, W.; Luo, Z. Pyrolysis Behaviors of Four Lignin Polymers Isolated from the Same Pine Wood. *Bioresour. Technol.* **2015**, *182*, 120–127. https://doi.org/10.1016/j.biortech.2015.01.127.

(87) Yuan, S.; Chen, X. L.; Li, J.; Wang, F. C. CO2 Gasification Kinetics of Biomass Char Derived from High-Temperature Rapid Pyrolysis. *Energy and Fuels* **2011**, *25* (5), 2314–2321. https://doi.org/10.1021/ef200051z.

(88) Fushimi, C.; Araki, K.; Yamaguchi, Y.; Tsutsumi, A. Effect of Heating Rate on Steam Gasification of Biomass. 1. Reactivity of Char. *Ind. Eng. Chem. Res.* **2003**, *42* (17), 3922–3928. https://doi.org/10.1021/ie030056c.

For Table of Contents Use Only

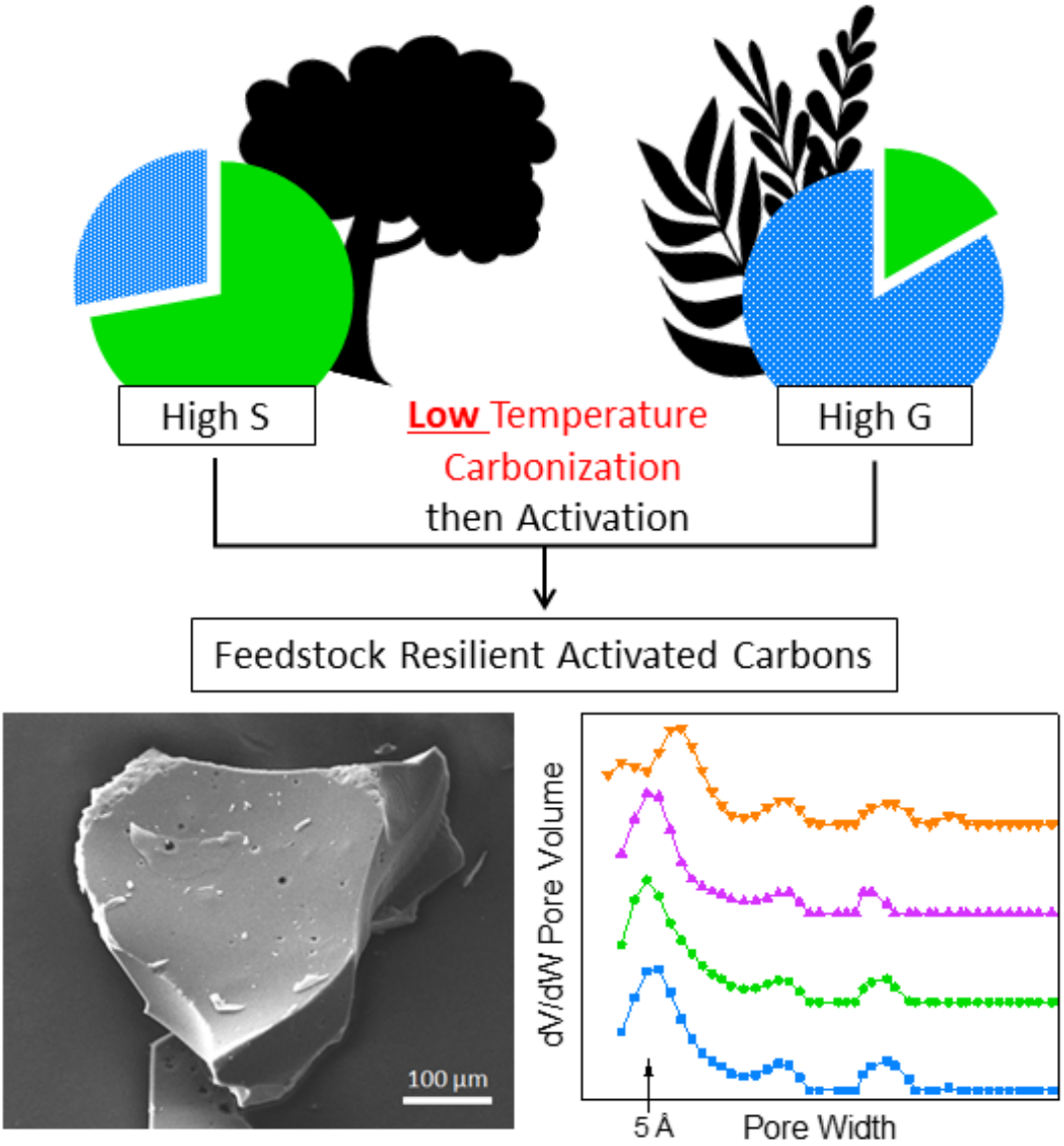

Synopsis

Utilizing low temperature carbonization conditions enables preparation of a feedstock-resilient activated carbon for hydrogen storage at a lower energy cost.